ELSEVIER

High-speed photography of fractures in weak snowpack layers

A. van Herwijnen [a], B. Jamieson [a,b,*]

[a]Dept. of Civil Engineering, University of Calgary, Canada
[b]Dept. of Geology and Geophysics, University of Calgary, Canada

Abstract

During the winters of 2002–2003 and 2003–2004, fractures in weak snowpack layers were recorded with a portable digital high-speed camera in the Columbia Mountains of British Columbia, Canada. Fractures were photographed at 250 frames per second in 21 compression tests, four rutschblock tests, three cantilever beam tests as well as on five skier-tested slopes. Theoretical slab avalanche release models generally assume propagation of a brittle shear fracture in an incompressible weak snowpack layer. However, displacement measurements of markers placed in the snow above the weak layer indicated that slope normal displacement (due to crushing of the weak layer) was directly caused by the fracture in the weak layer and independent of slope angle, whereas the slope parallel displacement following fracture was probably dependent on slope angle. Furthermore, displacement measurements from rows of markers placed in the snow above weak layers resulted in fracture speed measurements ranging from 17 to 26 m/s, in good agreement with the only other published fracture speed measurement known to the authors: 20 m/s.
© 2005 Elsevier B.V. All rights reserved.

Keywords: Slab avalanches; Fracture speed; Fracture propagation; Weak layer; Snowpack stratigraphy

1. Introduction

It is now widely accepted that the fractures that release slab avalanches initiate at a weak layer (or interface) underlying a cohesive slab (e.g. Schweizer et al., 2003). Theoretical models generally assume that slab avalanche release is caused by rapid propagation

of a brittle shear fracture in a weak snowpack layer, initiating from a pre-existing deficit zone or super weak zone (e.g. McClung, 1979, 1981, 1987; Bader and Salm, 1990). Field observations have shown that weak layers or interfaces are necessary for slab avalanching (e.g. Föhn, 1993). Field studies on spatial variability have demonstrated that the strength of a weak layer is not uniform over a slope (e.g. Stewart, 2002; Kronholm and Schweizer, 2003) but have not identified areas where the shear stress exceeds the shear strength. Traditionally, shear frames have been used to test the strength of weak snowpack layers and

* Corresponding author. Dept. of Civil Engineering, University of Calgary, Canada.
  E-mail address: bruce.jamieson@ucalgary.ca (B. Jamieson).

determine stability indices (e.g. Jamieson and Johnston, 1998) based on ratios of strength to stress. Fracture toughness of snow has also been recognized as being a relevant parameter for slab avalanching (e.g. McClung, 1981). Recently, field and laboratory measurements are beginning to produce toughness values and show its relation to snow parameters such as density and temperature (e.g. Kirchner et al., 2002; Schweizer et al., 2004).

Despite the progress that has been made to better understand the failure initiation and release process of a slab avalanche, there are still no consistent in situ measurements of propagating fractures in weak snowpack layers. However, such measurements are essential to verify theoretical models. A study on the dynamic response of the snow cover has shown that the additional stress introduced by a skier decreases with depth (Schweizer et al., 1995). In the same study, a video sequence of a fracture caused by rapid surface loading was analyzed. This was probably the first directly photographed observation of a fracture in a weak snowpack layer. Unfortunately, no further tests were reported. Johnson et al. (2004) used geophones placed on the snow surface on low angle terrain to measure the vertical displacement of the snow surface due to a propagating fracture in a weak snowpack layer. This was the first direct measurement on fracture propagating through a weak layer, resulting in a fracture speed of 20 m/s.

For the current study, a portable high-speed camera was used to photograph in situ fractures in weak snowpack layers in the Columbia Mountains in British Columbia, Canada. Fractures in various snowpack tests (compression, rutschblock and cantilever beam tests) and on skier-tested slopes were photographed at an interval of 4 ms in order to directly observe fractures in weak snowpack layers. The aim was to obtain displacement measurements at the time of fracture and also fracture speed measurements, which is one way to verify theoretical models.

2. Methods

2.1. Field tests

The portable high-speed camera (MotionMeter) that was used during the winters of 2002–2003 and

2003–2004 has a 658×496 pixel CCD array and an internal memory that can store up to 8.5 s of images at 250 frames per second. For transfer to a portable computer, the images were down-sampled to 344×264 pixels.

Fractures in weak snowpack layers were photographed in compression tests (CT) that were performed according to the Canadian snowpack observation standards (Canadian Avalanche Association, 2002). This test consists of an isolated 30 cm × 30 cm column of snow which is loaded from the snow surface by manually taping on a snow shovel (Fig. 1a). Due to the relatively small size of the test column, the compression test could not be used to analyze propagating fractures. However, these tests were useful in analyzing different types of fractures, classified according to the fracture characterization scheme introduced by Jamieson (1999) for classification of fractures by practitioners and refined by van Herwijnen and Jamieson (2003) (Table 1). In total, 22 fractures in 21 compression tests were photographed with the high-speed camera. In order to increase the contrast of the images, black powder (photocopy toner) was blown on the snow around the weak layer or black markers (rubber corks with a diameter of 24 mm) were carefully placed in the snow above and below the weak layer (Fig. 1).

Propagating fractures were photographed in larger tests such as the rutschblock test (RB), the cantilever beam test (CB) as well as on skier-tested slopes (ST). In rutschblock tests (Fig. 1b), a 1.5 m × 2 m block of snow was loaded by a skier (e.g. Föhn, 1987). Cantilever beam tests (Fig. 2a) were 30 cm wide and approximately 2 m long. The slab was undercut along the weak layer using a saw with a 2 cm wide cut (Fig. 2b). On skier-tested slopes, an up-slope trench, typically 4 m long, was dug prior to testing, in order to expose the weak layer for photography. In all these tests, black markers were inserted in the vertical snow wall above the weak layer to analyze the motion of the slab. The markers were placed 5 cm above the weak layer and a distance d apart (5, 10 or 20 cm). Markers were also placed below the weak layer. The camera was mounted horizontally on a tripod, aimed at the weak layer of interest and the test was performed until the weak layer fractured. Fractures were photographed in four rutschblock tests, three cantilever beam tests and
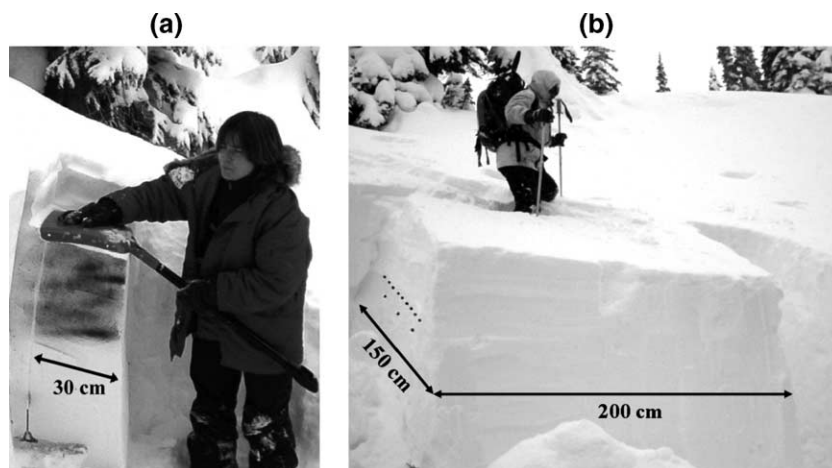
(a)   **(b)**

Fig. 1. Fractures in weak snowpack layers were photographed in compression tests (a) and rutschblock tests (b). Black powder was used to increase the contrast in most photographed compression tests. Markers were inserted in vertical snow wall above and below the weak layer to analyze the motion of the slab in rutschblock tests.

on five skier-tested slopes. All tested weak layers consisted of either buried surface hoar (SH), faceted crystals (FC) or depth hoar (DH).

Additionally, at each test site, a snow profile was observed to obtain information about hand hardness, crystal type, crystal size, layer thickness, temperature and density of the snow layers (Canadian Avalanche Association, 2002).

Table 1

Descriptive classification of fracture character in stability tests (van Herwijnen and Jamieson, 2003)

Fracture character	Code	Fracture characteristics
Progressive Compression	PC	Fracture usually crosses column with one loading step, followed by gradual compression of the layer with subsequent loading steps.
Resistant Planar	RP	Planar or mostly planar fracture that requires more than one loading step to cross column and/or block does not slide easily on weak layer.
Sudden Planar	SP	Planar fracture suddenly crosses column with one loading step and the block slides easily[a] on weak layer.
Sudden Collapse	SC	Fracture suddenly crosses column with one loading step and causes noticeable slope normal displacement.
Non-planar Break	B	Irregular fracture.

[a] Block slides off column on steep slopes. On low angle slopes, hold sides of block and note resistance to sliding.

2.2. Image analysis and fracture speed calculation

Particle tracking software (Crocker and Grier, 1996) was used to analyze the images of propagating fractures. A spatial bandpass filter identified the markers in the images and coordinates were assigned to the centroid of each marker. This was done for all the images so that the position of all markers was known at any given time. By 'connecting the dots' the trajectory for each marker was determined. When analyzing the images, a coordinate system with a slope parallel (x) and slope normal (y) axes was used (Fig. 2b). In such a coordinate system, a collapsing fracture results in slope parallel (Δx) and slope normal (Δy) displacement of the overlying slab. The displacement of a marker was calculated as the departure from the initial position:

$$\Delta x(t) = x(t) - X_0 \tag{1}$$

$$\Delta y(t) = y(t) - Y_0 \tag{2}$$

where the initial position (X_0, Y_0) was determined by averaging the position of the marker over 50 frames prior to movement.

The accuracy of the particle tracking software depends on the size and the quality of the images (i.e. signal to noise ratio). For each test, the accuracy ε was determined by calculating the standard deviation in the initial position of the markers. The accuracy
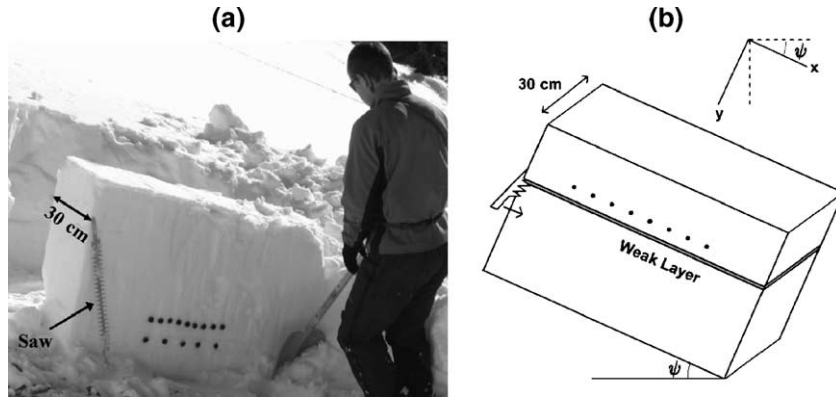
Fig. 2. The cantilever beam test was used to photograph propagating fractures. (a) Black markers were inserted in the vertical snow wall above the weak layer in a 30 cm wide and 2 m long cantilever beam. (b) The slab was undercut along the weak layer using a 2 cm wide saw. For analysis, a coordinate system with a slope parallel x and slope normal y component was used as shown for a slope angle ψ.

was typically on the order of 0.02 cm. However, during movement, uneven pixel clipping at the edges of the markers (Fig. 3) introduced additional scatter in the displacement data. A seven point moving average filter was found to be most effective in reducing these fluctuations in the displacement data without substantial loss of detail (Fig. 4).

For propagating fractures there is a retardation between the displacement of subsequent markers, as is shown schematically for Δy in Fig. 5a and b. For a given displacement Δy_*, the time t_i, corresponding to the time when $\Delta y_i(t) = \Delta y_*$ for Marker i, is expected to be proportional to the initial position X_{0i}. Assuming a constant fracture propagation velocity (i.e. $t_2 - t_1 = t_3 - t_2 = \ldots t_N - t_{N-1}$), the fracture speed $V_{\Delta y_*}$ is the slope of the line between X_{0i} and t_i (Fig. 5c) and is equal to the propagation speed of the advancing fracture. However, due to inaccuracies in the displacement data, a single value of Δy_* can lead to an inaccurate fracture speed calculation. To improve the accuracy, the fracture speed $V_{\Delta y_*}$ was calculated for a wide range of Δy_* values, sampled at an interval of $(\varepsilon/2)$ (Fig. 5d). An estimate of the propagation speed was then obtained by averaging the calculated fracture speed

$V_{\Delta y_*}$ for $\varepsilon < \Delta y_* \leq \Delta y_{max}/2$, and is referred to as $\overline{V_{\Delta y}}$. A maximum value of $\Delta y_{max}/2$ was chosen in order to account for any attenuation in the slope normal displacement (e.g. Fig. 6). Similarly, a fracture speed estimate $\overline{V_{\Delta x}}$ was calculated from the slope parallel displacement measurements. However, in most tests, the slab above the weak layer moved down-slope after the weak layer had fractured. Therefore, the slope parallel displacement of the markers did not reach a maximum value since slope parallel displacements
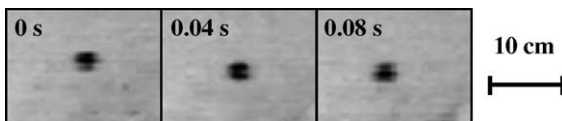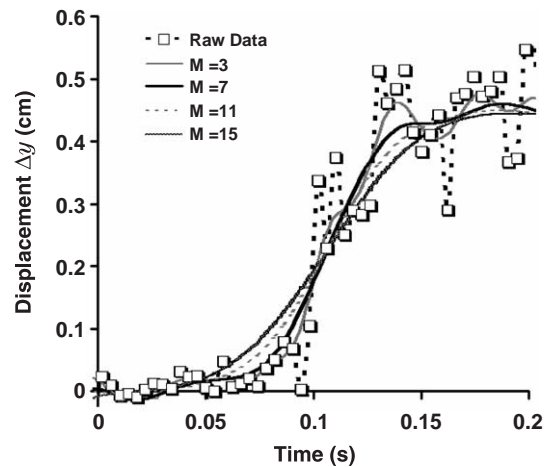

Fig. 3. Images of a moving marker at three different times showing uneven pixel clipping at the edges of the marker, leading to errors in the determination of the centroid of the marker.

Fig. 4. Example of raw slope normal displacement measurements and moving average curves of various degrees M. Scatter in the displacement curve, introduced by uneven pixel clipping, was reduced by these filters. A seven point moving average was most effective in reducing these displacement fluctuations without substantial loss of detail.
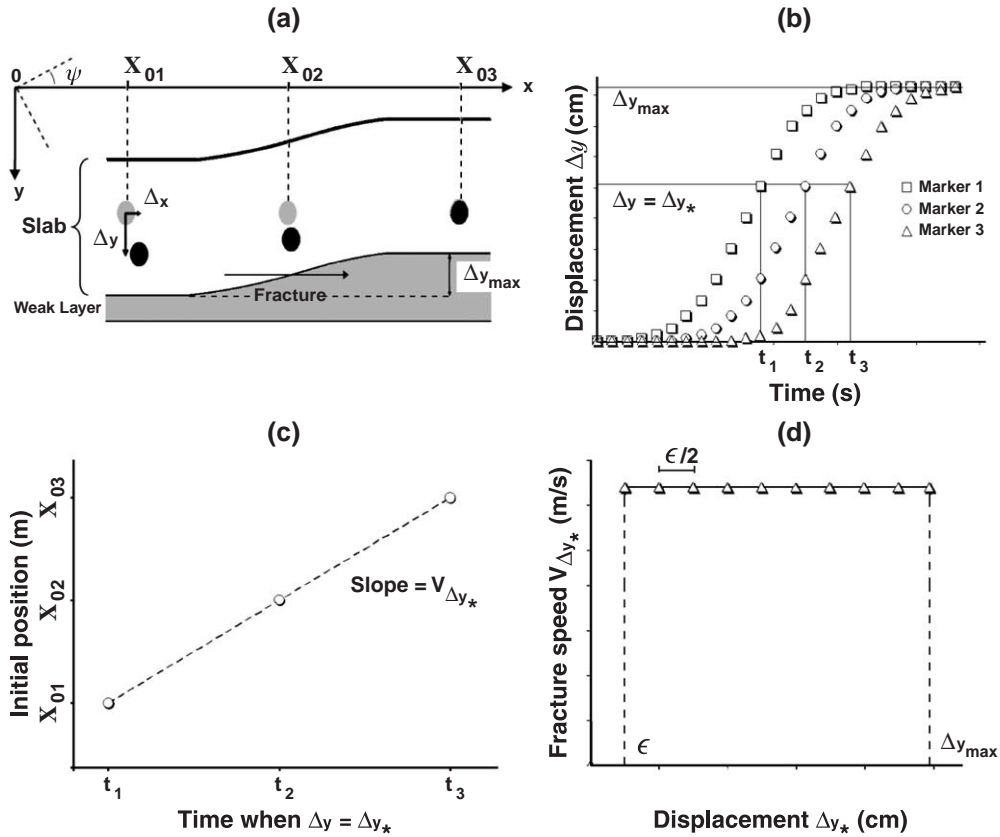
Fig. 5. Stages of the fracture speed calculations. (a) Schematic representation of the slope parallel (Δx) and slope normal (Δy) displacement of three markers due to a propagating collapsing fracture on a slope (not to scale). (b) Schematic slope normal displacement curves. The slope normal displacement reaches a maximum value of Δy_{max} after the weak layer has fractured. The time t_i, corresponding to the time when $\Delta y = \Delta y_*$ for Marker i, are used in the fracture speed calculation. (c) The propagation speed $V_{\Delta y_*}$ is equal to the slope of the line between the initial positions X_{0i} and the time t_i for a displacement of $\Delta y = \Delta y_*$, assuming a constant propagation velocity. (d) The fracture speed is calculated for a range of values of Δy_* sampled at an interval of $(\varepsilon / 2)$.

caused by the down-slope slab movement could not be separated from displacement caused by the fracturing of the weak layer. Nevertheless, in order to obtain fracture speed estimates from the slope parallel displacement, the same limits were used as for the calculation of $\overline{V_{\Delta y}}$.

3. Results

3.1. Observations of fractures in compression tests

Four fractures in compression tests were photographed with black markers in the snow wall above the weak layer (Table 2). A fracture in a buried surface hoar layer (CTA) that was judged as Sudden Planar (Table 1), tested on a level study site, resulted in a maximum slope normal displacement of 0.28 ± 0.05 cm, whereas the slope parallel displacement was undetectable. Three Sudden Collapse fractures in a weak layer consisting of faceted crystals were performed on a $30°$ slope. The measured Δy_{max} for these tests ranged from 1.3 ± 0.1 cm to 1.7 ± 0.1 cm and Δx did not level off as the test columns moved downslope. Therefore, the values of Δx_{max} in Table 2 for these tests are the average slope parallel displacements in the last frame, which are primarily affected by the length of the videos.

Fig. 6 shows images of the markers at the start and at the end of compression test CTC (Table 2), as well
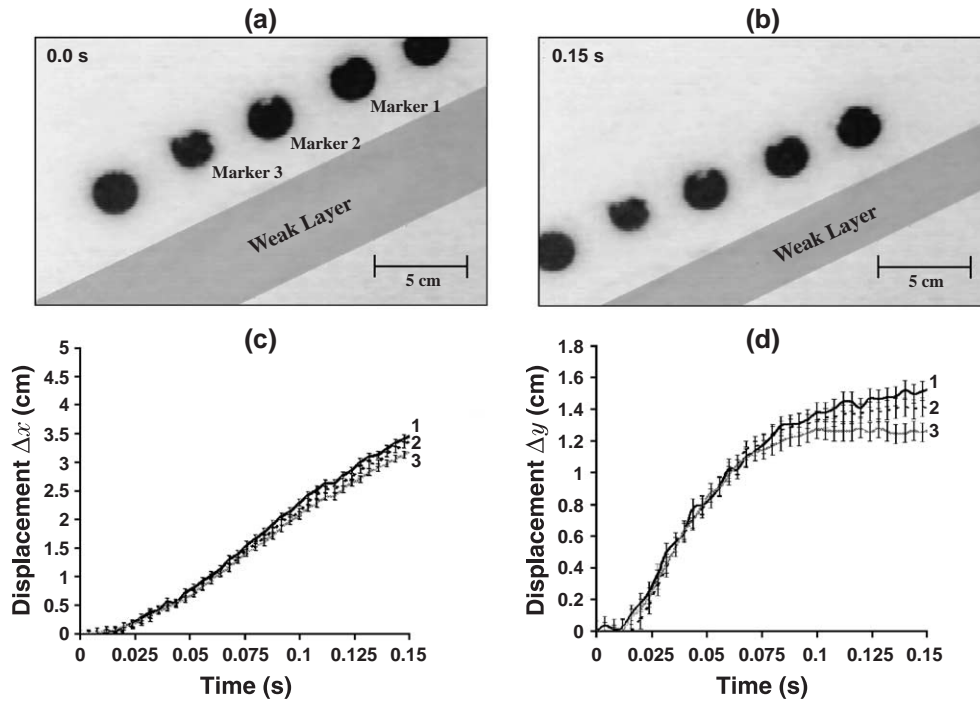
Fig. 6. (a) Image of markers at the start of compression test CTC. (b) Image of markers at the end of the compression test. (c) Slope parallel displacement. (d) Slope normal displacement. The accuracy of the displacement measurements for this test was 0.01 cm.

as the displacements Δx and Δy. The slope parallel displacement increased steadily after the weak layer fractured and the compression test column moved down-slope. The slope normal displacement on the other hand, increased steadily up to 0.8 cm, after which the rate of collapse decreased (i.e. attenuation) until an average maximum value of 1.3 ± 0.1 cm was reached after approximately 0.1 s. As seen in Fig. 6, the displacement of Marker 1 was largest. This was

Table 2
Measurements from photographed fractures in compression tests

Test	ψ	Char	F	h (cm)	ε (cm)	Δx_{max} (cm)	Δy_{max} (cm)
CTA	0	SP	SH	0.7	0.02	0.01 ± 0.04	0.22 ± 0.04
CTB*	30	SC	FC	5.5	0.02	3.4 ± 0.1	1.3 ± 0.1
CTC*	30	SC	FC	5.5	0.01	3.3 ± 0.1	1.7 ± 0.1
CTD*	30	SC	FC	5.5	0.1	4.7 ± 0.1	1.3 ± 0.1

Slope angle in degrees (ψ), observed fracture character (Char), weak layer crystal type (F) and weak layer thickness measured vertically (h) are given. Furthermore, the accuracy of the displacement measurements (ε), the average slope parallel displacement in the last frame (Δx_{max}) and the average maximum slope normal displacement after fracture (Δy_{max}) are shown. Tests in which the slab moved down-slope after fracture are marked with an asterisk.

caused by tilting of the compression test column after the weak layer had fractured and the column moved down-slope.

In the majority of the photographed compression tests, no markers were used, but black powder was blown on the snow to increase contrast. No quantitative analysis of these images can be done. Nevertheless, crushing of the weak layer was observed in each test (i.e. slope normal displacement), regardless of the fracture character. Furthermore, the mechanism that caused different fracture types (van Herwijnen and Jamieson, 2002) was observed in the images. For Progressive Compression (PC) and Sudden Collapse (SC) fractures, the fracture occurred through the thickness of the whole weak layer. In PC fractures, the crystals in the weak layer were rearranged after each loading step, resulting in progressive crushing of the weak layer. For SC fractures on the other hand, the critical loading step resulted in an obvious displacement of the overlying slab by a sudden and extensive rearrangement of the crystals throughout the weak layer. Images of the only recorded Resistant Planar fracture showed that the fracture occurred at the lower

interface of a weak layer due to rearrangement of the crystals at the interface, resulting in slope normal displacement of the overlying slab (<1 cm). Sudden Planar fractures were only photographed in weak layers composed of buried surface hoar crystals. The fractures appeared to occur due to rupturing of the bonds between the weak layer and the adjacent layers, as proposed by Jamieson and Schweizer (2000), causing the weak layer to collapse. These layers were thin (<1 cm) resulting in limited slope normal displacement of the overlying slab.

3.2. Observations of fractures on skier-tested slopes that were not triggered

Two skier-tested slopes that were photographed did not release a slab avalanche (Test A and B, Table 3). The images show that the skier fractured the weak layer as he pressed down on his skis while attempting to trigger the slab. These observations, one of which is described in detail below, show that a skier can fracture a weak layer without releasing a slab avalanche.

The displacement measurements for test A are shown in Fig. 7. The quality of the images was compromised by uneven illumination, resulting in an accuracy of only 1 mm. Markers 1 to 6 were displaced by the skier, whereas Markers 7 and 8 did not move. The distance over which the weak layer was fractured

was estimated from photos as being 3 ± 0.2 m. Markers were also placed under the weak layer but did not exhibit any detectable displacement (not shown).

Marker 1 was the closest to the skier's skis (approximately 70 cm) and consequently both Δx and Δy were the greatest for this marker: 9.6 ± 0.1 cm and 2.5 ± 0.1 cm, respectively. Furthermore, the displacement of the markers decreased with the distance from the skier (Fig. 7). The slope parallel displacement ranged from 9.6 ± 0.1 cm to 0.3 ± 0.1 cm and the slope normal displacement ranged from 2.5 ± 0.1 cm to 0.2 ± 0.1 cm for Marker 1 and Marker 6, respectively. The initial slope parallel distance between Marker 1 and Marker 6 was 100 ± 1 cm, resulting in a slope parallel strain of $9.3 \pm 0.1\%$. As seen in Fig. 7, the markers were in motion for 0.25 ± 0.05 s, leading to an approximate slope parallel strain rate of 0.37 ± 0.06 s^{-1}, well within the brittle range (e.g. Narita, 1980).

3.3. Observations of propagating fractures

Fracture speed estimates were obtained from 10 photographed propagating fractures. Information on these propagating fractures, as well as from the previous two skier-tested slopes, is given in Table 3. In the majority of photographed propagating fractures, the slab moved down-slope after the weak

Table 3
Measurements from photographed fractures in cantilever beam tests (CB), rutschblock tests (RB) and on skier-tested slopes (ST)

Test	Type of test	ψ	Char	F	h (cm)	H (cm)	ρ_{slab} (kg m^{-3})	ε (cm)	N	d (cm)	Δx_{max} (cm)	Δy_{max} (cm)	$\overline{V_{\Delta x}}$ (m/s)	$\overline{V_{\Delta y}}$ (m/s)
A	ST	34	SP	SH	2	62	105	0.1	6	20	9.6 to 0.3	2.5 to 0.2	–	–
B	ST	31	SP	SH	1.3	69	136	0.1	2	20	7.4 to 4.8	0.3 ± 0.1	–	–
C	CB	20	SP	SH	1.5	69	213	0.04	5	5	0.1 ± 0.05	0.4 ± 0.1	3 ± 2	20 ± 8
D	CB	20	SP	SH	1.5	69	213	0.02	5	5	0.06 ± 0.03	0.15 ± 0.05	5 ± 3	16 ± 6
E*	RB	19	SP	SH	1.5	69	213	0.03	5	5	1.97 ± 0.03	0.33 ± 0.03	18 ± 14	19 ± 7
F*	RB	21	SP	SH	1.5	69	213	0.01	5	5	3.06 ± 0.05	0.51 ± 0.02	2 ± 5	26 ± 7
G*	ST	32	SP	SH	2.1	49	175	0.05	5	20	4.2 ± 0.1	0.5 ± 0.1	21 ± 8	21 ± 6
H*	CB	34	SP	SH	0.7	85	193	0.02	6	10	1.82 ± 0.06	0.35 ± 0.05	5 ± 14	20 ± 5
I*	ST	33	SC	DH	5 to 10	42	199	0.06	5	20	3.6 ± 0.1	1.2 ± 0.1	33 ± 20	23 ± 6
J*	RB	37	SP	FC	0.4	53	105	0.03	5	20	7.8 ± 0.1	0.29 ± 0.04	30 ± 18	17 ± 4
K*	RB	40	SP	SH	0.8	90	158	0.05	6	10	3.2 ± 0.1	0.3 ± 0.1	21 ± 15	23 ± 5
L*	ST	44	SP	SH	0.8	94	132	0.08	5	20	3.6 ± 0.1	0.4 ± 0.1	30 ± 7	21 ± 8

Slope angle in degrees (ψ), observed fracture character (Char), weak layer crystal type (F), weak layer thickness measured vertically (h), depth of the weak layer measured vertically (H), the accuracy of the displacement measurements (ε), the number of markers that were displaced (N) and the marker separation (d) are given. The maximum slope parallel displacement Δx_{max}, the maximum slope normal displacement Δy_{max} and the average fracture speed $\overline{V_{\Delta x}}$ and $\overline{V_{\Delta y}}$ were derived from the seven point moving average displacement measurements of the markers. Tests in which the slab moved down-slope after fracture are marked with an asterisk.
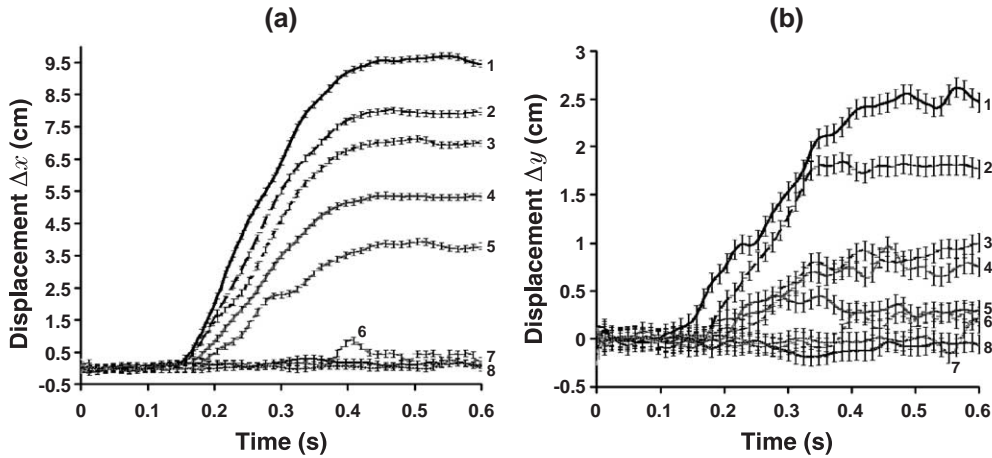
Fig. 7. Seven point moving average of the displacement of markers placed 5 cm above a buried surface hoar weak layer on a skier-tested slope that did not release a slab avalanche (test A). The Marker separation d was 20 cm and Marker 1 was closest to the skier (approximately 70 cm). (a) Slope parallel displacement. (b) Slope normal displacement. The accuracy of the displacement measurements for this test was 0.1 cm.

layer had fractured. The values of Δx_{max} therefore indicate the average slope parallel displacements of all markers in the last frame, and are larger than Δy_{max}. However, in two cantilever beam tests (tests C and D), the fracture propagated through the photographed section of the beam without propagating through the whole beam. Therefore, there was no down-slope sliding of the entire slab after the weak layer had fractured, and the slope parallel displacement of the markers reached a maximum value after the weak layer had fractured. In these tests, the average maximum slope parallel displacement (0.1 ± 0.05 cm and 0.06 ± 0.03 cm for tests C and D, respectively) was lower than the average maximum slope normal displacement (0.4 ± 0.1 cm and 0.15 ± 0.05 cm for tests C and D, respectively). Furthermore, the maximum slope normal displacement was similar for all surface hoar weak layers tested and showed no dependence on weak layer thickness before fracture ($N = 8$, Pearson $r = 0.30$, $p = 0.47$), whereas Δy_{max} was largest for the weak layer composed of depth hoar (test I).

In Fig. 8 the displacement of markers placed above the weak layer in cantilever beam test C is shown. Clearly, there is a retardation between the displacement of subsequent markers. However, due to inherent inaccuracies in the displacement measurements (Fig. 8), it was not possible to determine whether the propagation speed was constant or accelerated. Therefore, it was assumed that the propagation

speed was constant. As can be seen in Fig. 8, the maximum slope normal displacement for Marker 1 (0.52 ± 0.04 cm) was greater than that of Marker 5 (0.40 ± 0.04 cm), indicating that Δy_{max} decreased with the distance from the saw cut. Similarly, the maximum slope parallel displacement for Marker 1 (0.19 ± 0.04 cm) was greater than that of Marker 5 (0.11 ± 0.04 cm). This was likely due to a slight change in thickness of the weak layer or due to influences from the saw cut. However, this behavior was not observed in two other photographed cantilever beam tests (tests D and H).

The fracture speed calculations obtained from the seven point moving average slope parallel and slope normal displacements of the markers in cantilever beam test C are shown in Fig. 9. The values of $V_{\Delta y*}$ are relatively constant for $\Delta y*$ between 0.04 ($= \varepsilon$) and 0.2 cm ($= \Delta y_{max}/2$). For values of $\Delta y*$ larger than 0.2 cm, the calculated fracture speed $V_{\Delta y*}$ decreases. On the other hand, the fracture speed calculated from the slope parallel displacement was much lower and could only be calculated for a limited range of displacement values. Averaging the values of $V_{\Delta y*}$ for $0.04 \leq \Delta y* \leq 0.2$ cm yields a fracture speed of $\overline{V_{\Delta y}} = 22 \pm 8$ m/s, whereas $\overline{V_{\Delta x}} = 4 \pm 2$ m/s for $0.04 \leq \Delta x* \leq 0.1$.

As can be seen in Table 3, the fracture speed $\overline{V_{\Delta x}}$ was highly variable, ranging from 2 ± 5 m/s for test F to 33 ± 20 m/s for test I. The fracture speed obtained from the slope normal displacement, on the other
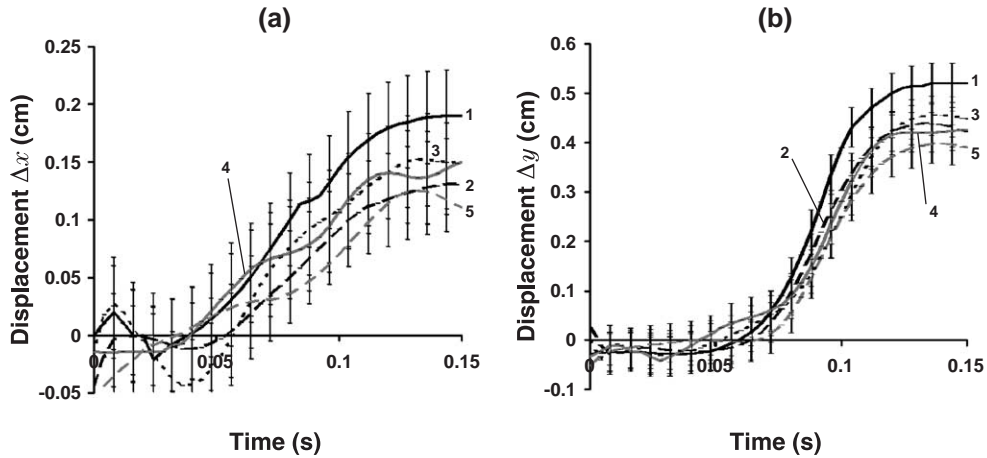
(a)

(b)

Fig. 8. Seven point moving average of the displacement of markers placed above a buried surface hoar weak layer in a cantilever beam test (test C). The marker separation d was 5 cm. (a) Slope parallel displacement. (b) Slope normal displacement. The accuracy of the displacement measurements for this test was 0.04 cm.

hand, was more consistent between the different tests. The mean measured fracture speed was 21 ± 3 m/s. As seen in Fig. 10, there was a trend for the fracture speed to increase with increasing Δy_{max}, although the correlation between $\overline{V_{\Delta y}}$ and Δy_{max} was not significant ($N=10$, Pearson $r=0.53$, $p=0.12$). However, when only weak layers composed of buried surface hoar are considered, there was a significant positive correlation between $\overline{V_{\Delta y}}$ and Δy_{max} ($N=9$, Pearson $r=0.74$, $p=0.02$).

4. Discussion

Photography of different types of fractures in compression tests has shown that fracturing of weak layers caused slope parallel and slope normal displacement of the overlying slab. The amount of slope parallel displacement at the time of fracture appeared to be dependent on slope angle since markers in a compression test performed on a level study site (CTA) did not display any detectable slope parallel displacement. On the other hand, markers in cantilever beam tests on a
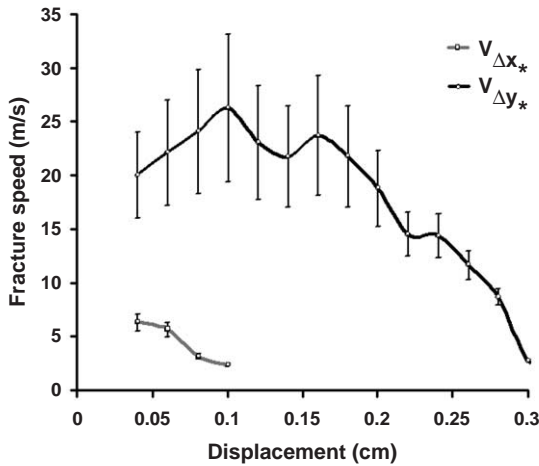

Fig. 9. Fracture speed measurements obtained from the displacement shown in Fig. 8. The accuracy was $\varepsilon=0.04$ cm and the maximum displacements after fracture were $\Delta y_{max}=0.4 \pm 0.1$ cm and $\Delta x_{max}=0.1 \pm 0.05$ cm.
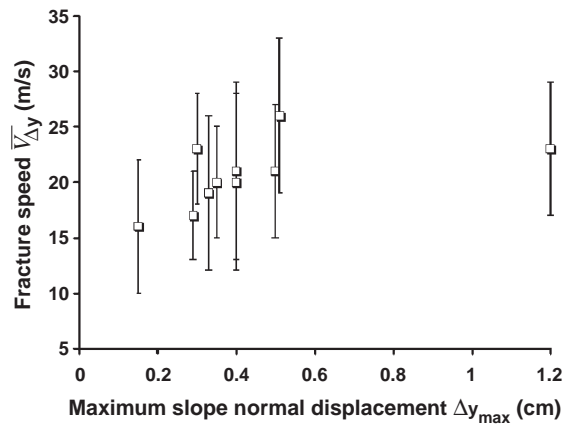

Fig. 10. Fracture speed measurements obtained from the slope normal displacement ($\overline{V_{\Delta y}}$) by maximum slope normal displacement at the end of fracture (Δy_{max}). The rightmost point is for the depth hoar layer (test I) and the other points are for layers of buried surface hoar.

20° slope (tests C and D), where the fracture propagated approximately 0.5 m beyond the edge of the saw cut without releasing the overlying slab, were displaced in both directions. However, Δy was larger than Δx. This is consistent with the idea of free fall motion of the slab just after the fracture, in which case the slope parallel displacement due to fracture is equal to $\Delta y \tan\psi$.

Results from cantilever beam tests (tests C, D and H) show that the slope normal displacement was caused by the fracture of the weak layer and not by compaction of the snow due to external loading on the snow surface, since in cantilever beam tests no external load was applied on the slab. The weak layer fractured due to stress concentration at the edge of the saw cut caused by the weight of the unsupported slab causing the fracture to propagate beyond the saw cut. Therefore, the trajectories of the markers only reflect the response of the slab to the propagating fracture.

Slope normal displacement was observed in all fractures, regardless of slope angle or fracture character. It was greatest for Sudden Collapse fractures (CTB, CTC, CTD and test I), which are typically associated with weak layers composed of faceted crystals and depth hoar (van Herwijnen and Jamieson, 2002). Schweizer et al. (1995) report deformation measurements from a rammrutsch test, resulting in a slope normal displacement of 0.47 cm at the time of fracture. Field measurements (Johnson, 2000) showed that the average vertical displacement of the slab at whumpf sites (i.e. fracture propagation on low angle terrain without slab avalanche release) varied from 0.08 to 1.0 cm. These values are comparable to the present results for the maximum slope normal displacement, which ranged from 0.15 to 1.7 cm.

Displacement measurements on skier-tested slopes that did not release a slab avalanche (tests A and B) showed the dynamic deformation a skier has on the snowpack. The skier-induced deformation decreased with distance since displacements for markers farther away from the skier were less. The maximum measured slope normal displacement in test A was 2.3 ± 0.1 cm, much larger than the measured values for propagating fractures shown in Table 3, and larger than the weak layer thickness (2 cm). Moreover, the displacement of markers placed under the weak layer was undetectable. This indicates that the slope normal displacement was caused by fracturing of the weak

layer, which was clearly observed in the video, as well as by slope normal compaction of snow layers above the primary weak layer. Furthermore, there was also slope parallel snow compaction caused by compressive fractures in the slab, which were observed throughout the slab after the test was performed.

These results show that skiers can fracture weak layers without releasing a slab avalanche. Theoretical estimates of critical crack size for self-propagating fractures range from 0.1 to approximately 2 m (e.g. Kirchner et al., 2002; Bazant et al., 2003; Schweizer et al., 2003). From photographs taken before and after a ski-test (test A), the distance over which the weak layer fractured was estimated at 3.0 ± 0.2 m, larger than these theoretical predictions for the minimum size for self-propagating fractures. This indicates the importance of slab properties for fracture propagation. In itself, a large fracture in a weak layer is not sufficient for fracture propagation and slab avalanche release (Table 3).

Consistent fracture speed measurements, with a relatively large measurement error, were obtained from the slope normal displacement measurements. However, due to inaccuracies in the displacement measurements, it was not possible to determine whether the propagation was stationary or accelerated. Furthermore, fracture speed measurements from the slope parallel displacement did not result in consistent propagation speed values. Therefore, the fracture speed measurements should be considered cautiously. Nevertheless, the measured fracture speed $\overline{V_{\Delta y}}$ ranged from 17 to 26 m/s, with a mean of 21 m/s. Furthermore, despite the fact that these fracture speed measurements were obtained from tests of different sizes and with different loading methods, the $\overline{V_{\Delta y}}$ results showed no dependence on the test method. Also, these fracture speed values are in good agreement with the only other published fracture speed measurement known to the authors (20 m/s; Johnson et al., 2004) which was obtained from measurements over a distance of 8 m. Finally, even though there are limited data, there was a significant positive correlation between the fracture speed and Δy_{max} for weak layers composed of buried surface hoar. This suggests that the slope normal displacement (due to crushing of the weak layer) plays an important role in the fracturing process of weak snowpack layers and thus the initiation of slab avalanches.

Traditionally, avalanche release models have not included any slope normal displacement (Bader and Salm, 1990; McClung, 1979, 1981). The incompressible weak layer is assumed to fracture in slope parallel shear. On the other hand, a recent theory proposed by Johnson (2000) for fracture propagation on low angle terrain is based on compressive fracture of the weak layer. Energy is transferred through the overlying slab by means of a flexural wave, progressively compressing the weak layer. The present results suggest that a similar theory could be applicable for fracture propagation on a slope since slope normal displacement of the slab was observed in all tests, regardless of slope angle.

5. Conclusions

A portable high-speed camera was used to directly observe in situ fractures in weak snowpack layers at 250 frames per second. The mechanisms that cause different types of fractures were observed in compression tests. Furthermore, the use of markers placed in the snow wall above the weak layer allowed for detailed analysis of the displacement of the slab caused by the fracturing weak layer. Displacement measurements, with a typical accuracy of 0.02 cm, showed that fracturing of weak snowpack layers was associated with slope parallel and slope normal displacement of the overlying slab. Slope normal displacement, which ranged from 0.1 to 1.7 cm, was observed in all fractured weak layers, independent of slope angle, and comparable to previously published results. On the other hand, slope parallel displacement caused by the fracture of the weak layer was probably dependent on slope angle, as expected for free fall motion of the slab.

Photography of two skier-tested slopes that did not release slab avalanches showed that the snow deformation due to the skier decreased with distance and both slope normal and slope parallel compaction of the overlying slab were observed. Furthermore, the videos show that skiers can fracture a weak layer over distances greater than 1 m in the down-slope direction without releasing a slab avalanche.

Fracture speed measurements were obtained from 10 photographed propagating fractures. These data should be considered cautiously, since it was not possible to determine whether the fracture was accelerated or not. However, the average propagation speed $\overline{V}_{\Delta y}$ were comparable in all tests and of the order of 20 m/s, in good agreement with the only other published fracture speed measurement.

Acknowledgments

References

Bader, H.P., Salm, B., 1990. On the mechanics of snow slab release. Cold Regions Science and Technology 17, 287–300.

Bazant, Z.P., Zi, G., McClung, D., 2003. Size effect law and fracture mechanics of the triggering of dry snow slab avalanches. Journal of Geophysical Research 108 (B2), 2119.

Canadian Avalanche Association, 2002. Observation Guidelines and Recording Standards for Weather, Snowpack and Avalanches. Canadian Avalanche Association, Revelstoke, Canada.

Crocker, J.C., Grier, D.G., 1996. Methods of digital video microscopy for colloidal studies. Journal of Colloid and Interface Science 179 (1), 298–310.

Föhn, P.M.B., 1987. The rutschblock as a practical tool for slope stability evaluation. International Association of Hydrological Sciences Publication 162, 223–228.

Föhn, P.M.B., 1993. Characteristics of weak snow layers and interfaces. Proceeding of the International Snow Science Workshop, Breckenridge, Colorado, USA, 4–8 October 1992, pp. 160–170.

Jamieson, J.B., 1999. The compression test—after 25 years. The Avalanche Review 18 (1), 10–12.

Jamieson, J.B., Johnston, C.D., 1998. Refinements to the stability index for skier-triggered slab avalanches. Annals of Glaciology 26, 296–302.

Jamieson, J.B., Schweizer, J., 2000. Texture and strength changes of buried surface-hoar layers with implications for dry snow-slab avalanche release. Journal of Glaciology 46 (152), 151–160.

Johnson, B.C., 2000. Remotely triggered slab avalanches. MSc. Thesis, Dept. of Civil Engineering, University of Calgary, Calgary, Canada.

Johnson, B.C., Jamieson, J.B., Stewart, R.R., 2004. Seismic measurement of fracture speed in a weak snowpack layer. Cold Regions Science and Technology 40 (1–2), 41–45.

Kirchner, H.O.K., Michot, G., Schweizer, J., 2002. Fracture toughness of snow in shear and tension. Scripta Materialia 46, 425–429.

Kronholm, K., Schweizer, J., 2003. Snow stability variation on small slopes. Cold Regions Science and Technology 37 (3), 453–465.

McClung, D.M., 1979. Shear fracture precipitated by strain softening as a mechanism of dry slab avalanche release. Journal of Geophysical Research 84 (87), 3519–3525.

McClung, D.M., 1981. Fracture mechanical models of dry slab avalanche release. Journal of Geophysical Research 86 (11), 10783–10790.

McClung, D.M., 1987. Mechanism of snow slab failure from a geotechnical perspective. International Association of Hydrological Sciences Publication 162, 475–508.

Narita, H., 1980. Mechanical behavior and structure of snow under uniaxial tensile strength. Journal of Glaciology 26 (94), 275–283.

Schweizer, J., Schneebeli, M., Fierz, C., Föhn, P.M.B., 1995. Snow mechanics and avalanche formation: field experiments on the dynamic response of the snow cover. Surveys in Geophysics 16, 621–633.

Schweizer, J., Jamieson, J.B., Schneebeli, M., 2003. Snow avalanche formation. Reviews of Geophysics 41 (4), 1016.

Schweizer, J., Michot, G., Kirchner, H.O.K., 2004. On the fracture toughness of snow. Annals of Geology 38, 1–8.

Stewart, K.W., 2002. Spatial variability of slab stability within avalanche start zones. MSc. Thesis, Dept. of Geology and Geophysics, University of Calgary, Calgary, Canada.

van Herwijnen, A.F.G., Jamieson, J.B., 2002. Interpreting fracture character in stability tests. In: Stevens, J.R. (Ed.), Proceedings of 2002 International Snow Science Workshop in Penticton, Canada. BC Ministry of Transportation, Victoria, Canada, pp. 514–520.

van Herwijnen, A., Jamieson, J.B., 2003. An update on fracture character in stability tests. Avalanche News, vol. 66. Canadian Avalanche Association, Revelstoke, Canada, pp. 26–28.